

## NATURAL HAZARDS

# Citizen seismology helps decipher the 2021 Haiti earthquake

E. Calais<sup>1,2,3,4\*</sup>, S. Symithe<sup>3,5</sup>, T. Monfret<sup>2,3,6</sup>, B. Delouis<sup>2,3</sup>, A. Lomax<sup>7</sup>, F. Courboulex<sup>2,3</sup>, J. P. Ampuero<sup>2,3</sup>, P. E. Lara<sup>2,8</sup>, Q. Bletery<sup>2,3</sup>, J. Chèze<sup>2,3</sup>, F. Peix<sup>2,3</sup>, A. Deschamps<sup>2,3</sup>, B. de Lépinay<sup>2,3</sup>, B. Raimbault<sup>1</sup>, R. Jolivet<sup>1,4</sup>, S. Paul<sup>2,3,5</sup>, S. St Fleur<sup>3,5</sup>, D. Boisson<sup>3,5</sup>, Y. Fukushima<sup>9</sup>, Z. Duputel<sup>10</sup>, L. Xu<sup>11</sup>, L. Meng<sup>11</sup>

On 14 August 2021, the moment magnitude ( $M_w$ ) 7.2 Nippes earthquake in Haiti occurred within the same fault zone as its devastating 2010  $M_w$  7.0 predecessor, but struck the country when field access was limited by insecurity and conventional seismometers from the national network were inoperative. A network of citizen seismometers installed in 2019 provided near-field data critical to rapidly understand the mechanism of the mainshock and monitor its aftershock sequence. Their real-time data defined two aftershock clusters that coincide with two areas of coseismic slip derived from inversions of conventional seismological and geodetic data. Machine learning applied to data from the citizen seismometer closest to the mainshock allows us to forecast aftershocks as accurately as with the network-derived catalog. This shows the utility of citizen science contributing to our understanding of a major earthquake.

On 14 August 2021, a moment magnitude ( $M_w$ ) 7.2 earthquake struck the southern peninsula of Haiti (Fig. 1A), leaving ~2500 people dead, 13,000 injured, at least 140,000 houses destroyed or damaged, and a number of water, sanitation, and health facilities severely affected (1). Because the earthquake affected an area that is mostly rural, with low population density, its impact was much lower than the smaller but devastating 12 January 2010  $M_w$  7.0 Haiti event (2–4). Most of the damage and casualties were concentrated in the populated cities of Les Cayes and Jérémie (Fig. 1B), but hard-to-reach rural communities also took a hit, in a context aggravated by the tropical storm that followed the event and chronic insecurity complicating field access from the capital city. In spite of these difficulties, and in the absence of an operational national network of conventional seismic stations, nearby seismological data were readily available during and after the earthquake because of a citizen seismology effort using inexpensive and low-

maintenance “Raspberry Shake” (RS) seismic stations hosted by volunteers (5–7) (Fig. 1) [see (8), section 1]. This project had two original goals. The first was to install simple but scientifically useful seismological sensors in the homes of citizens to improve the dissemination of seismological information to the public, increase earthquake awareness, and promote grassroots protection initiatives (8). The second goal was to complement the national broadband seismological network, a high-technology system difficult to operate and maintain in a development context with a chronic lack of state resources. This citizen-based seismic network bears similarities to the Quake Catcher and Community Seismic networks deployed in California (9, 10), although these use accelerometers only and are deployed in a region already well covered with conventional seismic stations. The 14 August 2021 earthquake and its aftershock sequence are an important test of the applicability of low-cost, citizen-hosted seismometers to provide scientifically relevant data for rapid response to a major earthquake.

The 2021 Nippes earthquake occurred within the Caribbean–North American plate boundary (Fig. 1A), where the two plates are converging obliquely at a speed of ~2 cm/year (11). The convergence component of plate motion is accommodated by the underthrusting of the North American oceanic lithosphere along the Puerto Rico Trench–North Hispaniola Fault, and the left-lateral component is accommodated by the Septentrional and Enriquillo strike-slip fault zones (12–14). The Enriquillo fault zone is considered the source of at least three major historical earthquakes occurring in 1701 [intensity magnitude ( $M_I$ ) 6.6], 1751 ( $M_I$  7.4), and 1770 ( $M_I$  7.5) and a fourth, smaller earthquake in 1860 with  $M_I$  6.3 (15, 16) (Fig. 1A).

It was also the locus of the devastating  $M_w$  7.0 earthquake of 12 January 2010. The epicentral region of the 2021 Nippes earthquake experienced two major events in 1952 ( $M_w$  6.1) and 1953 ( $M_w$  6.0) (17) and recurring clusters of smaller felt events, for example, the one in 2015 (18).

The mainshock of the 2021 Nippes earthquake was detected and characterized within minutes as  $M_w$  7.2, consistent across most seismological agencies; this was 40% more energetic than the 2010 event, and with a source mechanism combining strike-slip and reverse faulting (19). It was recorded by five seismometers in Haiti: three RS stations hosted by citizens and two conventional stations in Port-au-Prince ~120 km from the epicenter, one US Geological Survey (USGS) accelerometer in the American embassy, and one educational broadband instrument in a high school (20). RS station R50D4, located 21 km from the epicenter (Fig. 1B), includes accelerometric sensors that recorded the mainshock without saturation with a maximum peak ground acceleration of 0.33 g on its north-south component (Fig. 2A). The high acceleration values for pseudo-periods lower than 0.5 s (Fig. 2C) [see (8), section 2] likely explains the severity of damages observed in the epicentral area in houses that, for the most part, were not built to earthquake-resistant standards. Spectral acceleration with 5% damping slightly exceeds the current Haiti building code (21, 22) (Fig. 2C), indicating that even constructions built to current standards were exposed to an unexpectedly high hazard.

We determined a source mechanism for the mainshock using a linear finite-source model and the waveform inversion of data from conventional seismic stations at regional distance plus the near-source three-component accelerometric record from RS station R50D4 (Fig. 2B) [see (8), section 3]. The mechanism, consistent with global seismological agencies (19), combines 45% of strike-slip and 55% of reverse moment release, with an east-west trending nodal plane consistent with the local strike of the Enriquillo fault and dipping 60° to the north (Fig. 1B). The optimal centroid source depth was 6 km, indicating that most of the seismic moment was released at shallow depth. The citizen network detected two events of specific interest in the near vicinity of the mainshock. A possible foreshock on 6 April 2021, local magnitude ( $M_l$ ) 4.5, coincides with the mainshock location, with a similar source mechanism (Fig. 1B). A substantial aftershock (08/25,  $M_l$  4.6) detected by four RS stations is located within a few kilometers of the mainshock with a purely reverse mechanism (Fig. 1B). The three-component accelerometric recordings of the RS instruments were too noisy to be exploited at low frequency for these two smaller events, but their vertical velocimetric

<sup>1</sup>Département de Géosciences, École Normale Supérieure, CNRS UMR 8538, PSL Université, Paris, France. <sup>2</sup>Université Côte d'Azur, Institut de Recherche pour le Développement, Centre National de la Recherche Scientifique, Observatoire de la Côte d'Azur, Géozur, Valbonne, France. <sup>3</sup>CARIBACT Joint Research Laboratory, Université d'État d'Haïti, Université Côte d'Azur, Institut de Recherche pour le Développement, Port-au-Prince, Haïti. <sup>4</sup>Institut Universitaire de France, Paris, France. <sup>5</sup>URGéo, Faculté des Sciences, Université d'État d'Haïti, Port-au-Prince, Haïti. <sup>6</sup>Barcelona Center for Subsurface Imaging, Institut de Ciències del Mar (ICM), CSIC, Barcelona, Spain. <sup>7</sup>Alomax Scientific, Mouxans Sartoux, France. <sup>8</sup>Instituto Geofísico del Perú, Lima, Perú. <sup>9</sup>International Research Institute of Disaster Science, Tohoku University, Sendai, Japan. <sup>10</sup>Observatoire Volcanologique du Piton de la Fournaise, Université de Paris, Institut de Physique du Globe de Paris, CNRS, Paris, France. <sup>11</sup>Department of Earth, Planetary and Space Sciences, University of California, Los Angeles, CA, USA. \*Corresponding author. Email: eric.calais@ens.fr

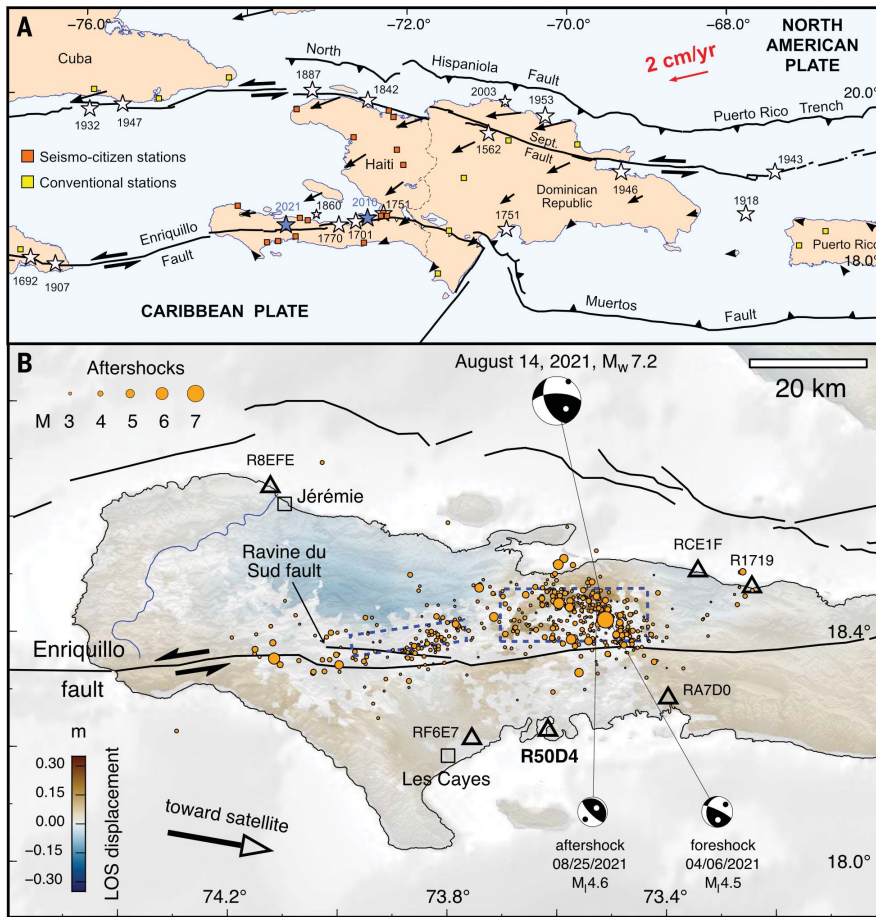


**Fig. 1. Seismotectonic context of the 2021 Nippes earthquake.** (A) Major active faults of the Caribbean–North America plate boundary zone with historical earthquakes (16) (stars) and Global Positioning System (GPS) velocities (black arrows) with respect to the Caribbean plate (11). (B) Relocated aftershock sequence (14 August to 9 September 2021) on top of a descending Sentinel interferogram spanning 3 to 8 August 2021. Triangles show citizen-hosted seismometers spanning the epicentral area. Line-of-sight (LOS) ground displacement north of the Enriquillo fault shows motion toward the satellite in the epicentral region (brown) and away from the satellite along the western part of the rupture (blue). Such reversal of the sense of motion along the LOS direction indicates substantial vertical motion in the epicentral region and almost pure horizontal, left-lateral motion to the west. Gray areas are not sufficiently coherent to ensure reliable phase unwrapping.

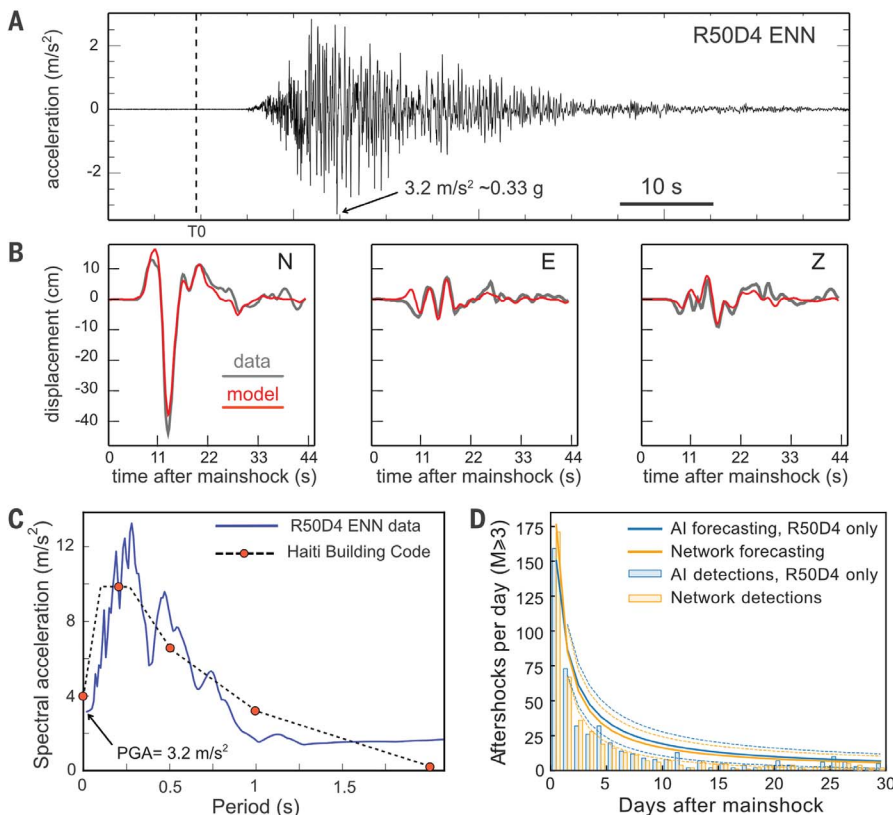


**Fig. 2. Data and inferences from citizen station R50D4, 21 km from the 2021 Nippes earthquake rupture.** (A) Signal in acceleration of the north component (channel ENN), which recorded a peak ground acceleration (PGA) of 0.33 g. Vertical line labeled T0 indicates the earthquake origin time. (B) Waveform fitting of the three components integrated to displacement and bandpass filtered between 0.06 and 0.5 Hz (N: north, E: east, Z: vertical up). The gray line is the observed signal, and the red line is the signal computed with the kinematic finite source model (Fig. 3B). (C) Spectral acceleration with 5% damping (blue line) of the north-south component of ground acceleration at the station (Fig. 1B). Red dots indicate the spectral values derived from the Haitian building code for the city of Les Cayes, closest to R50D4 and at the same distance from the rupture. The dashed line is drawn for visual interpretation but is not indicated in the code. Ground motion was stronger than expected for some frequency bands. (D) Detection and forecasting of aftershocks of magnitude >3 using the catalog derived from the whole network (orange) and from a single station (R50D4, blue). Histograms show detections, solid lines show forecast based on fitting an Omori-Utsu law to the first 12 hours of data, with their 95% confidence intervals indicated by dashed lines.

Downloaded from https://www.science.org on June 18, 2024

component contributed to the waveform inversion.

As of 9 September 2021, the citizen-based seismic network, together with regional conventional seismic stations located >120 km from the epicenter, detected 1031 aftershocks within a magnitude range of  $M_1$  1.4 to 5.8, with

a completeness magnitude around  $M_1$  2.8. For comparison, 37 aftershocks are available for the same period in the global USGS catalog (23), which targets  $M_{4.5+}$  earthquakes only outside of the United States. We precisely relocated the mainshock and its aftershocks using manual (70% of events) and automatic

P-wave and S-wave arrival picks, source-specific station terms, and waveform similarity (24), with estimated error in absolute positions of 5 to 8 km and relative positions between nearby events of as little as 2 km [see (8), section 4]. We show the 732 higher-quality aftershock locations in Figs. 1B and 3A. We used only P-wave arrivals for the precise mainshock relocation because S-wave arrivals for large events are hidden in the P-wave train, and obtained the hypocenter at 18.42°N/73.51°W and 19 km depth.

Aftershocks are mostly located to the north of the Enriquillo fault (Figs. 1B and 3A), with the densest activity extending ~50 km east-west in two separate clusters: an eastern northwest-oriented cluster with ~4- to 20-km depth range, an ~10 × 25 km<sup>2</sup> area and overall dip to the north-northeast, containing the mainshock hypocenter at its base, and a western northeast-oriented cluster with an ~5 × 15 km<sup>2</sup> area and most events shallower than ~10 km depth. The western cluster merges westward into a sparse, east-west trend of events extending up to ~30 km along the Enriquillo fault zone, giving a total east-west extent of the main aftershock activity of as much as 80 km. Relocation without the citizen-based seismic network gives almost no depth constraint and produces a featureless cloud of epicenters of ~80 km extent and shifted ~20 km northeast of the centroid of the precisely located seismicity clusters.

The real-time detection of a large number of aftershocks permitted by the citizen-based seismic network allowed us to forecast their decay rates in a timely manner, information useful to the local population and emergency responders. The Reasenber-Jones method (25) applied to the first 12 hours of the aftershock catalog shows a good match between the observed and forecast aftershock rates, which agree within 95% confidence over a 25-day interval [see (8), section 5]. In addition, we used a machine-learning (ML) approach to build an independent aftershock catalog using a single RS station (R50D4) [see (8), section 5]. These two independent catalogs are in good agreement, as well as the aftershock forecasts derived from each of them (Fig. 2D). This indicates that a single, well-located RS can provide the same forecast as the full network, maybe even a better one at very early times (fig. S6). This highlights the potential of low-cost instrumentation combined with ML for earthquake risk reduction in seismically active regions with limited resources.

We computed a kinematic finite fault-slip model using regional broad-band and strong-motion data, including near-field data from the R50D4 accelerometer (Fig. 3B) [see (8), section 6]. The rupture propagated unilaterally from the hypocenter westward over a distance of 50 to 60 km, at an average velocity of

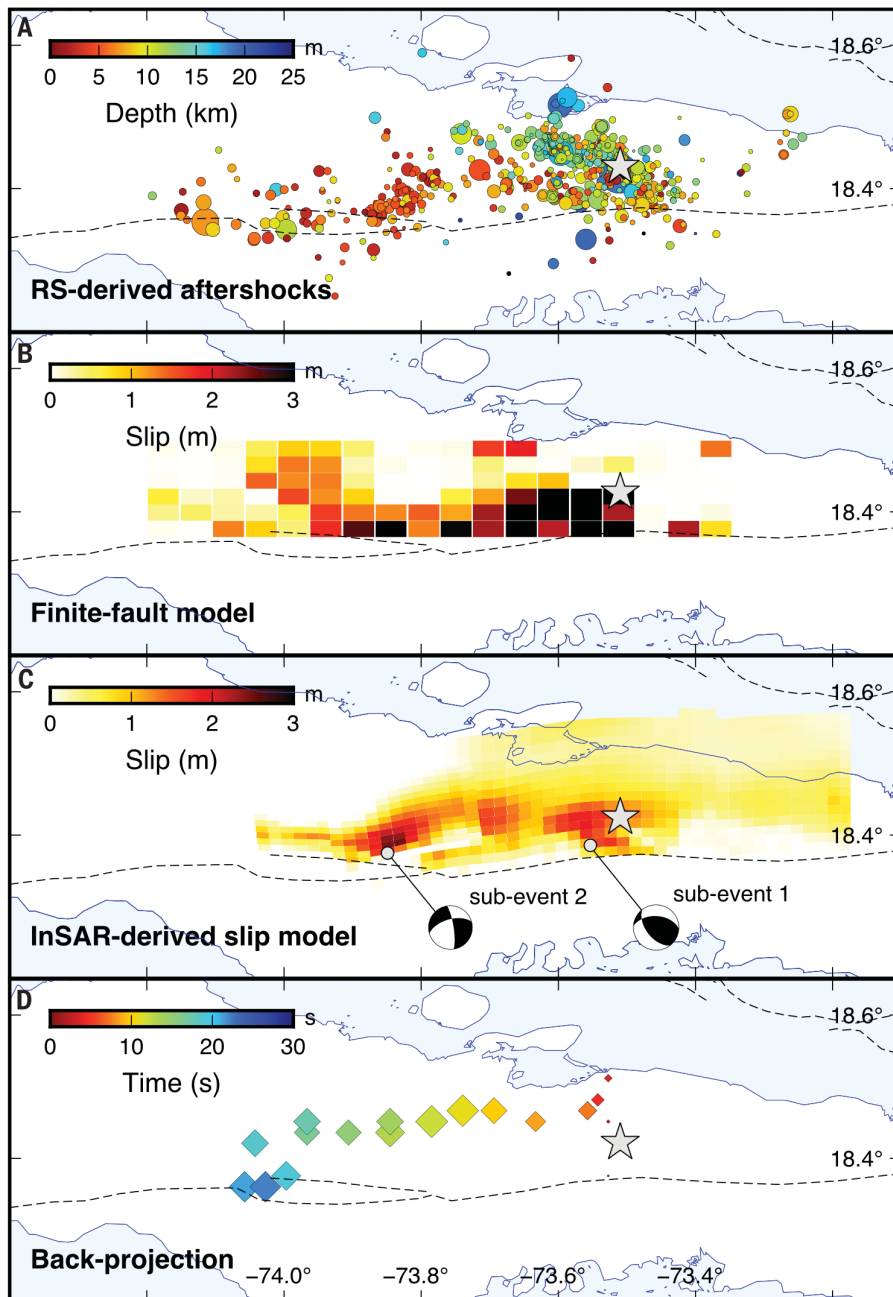


**Fig. 3. Comparison between aftershock locations using citizen-hosted seismometers and the mainshock source mechanism.** (A) Aftershock catalog after precise relocation with the 732 higher-quality events (14 August to 9 September 2021). (B) Kinematic finite fault model from an inversion of local and regional seismic stations. (C) Slip distribution inferred from InSAR data. The focal mechanisms derived from long-period modeling with two point sources are shown. (D) High-frequency (1 Hz) radiation sources (diamonds) from teleseismic back-projection source imaging. Symbol size is proportional to their relative energy and colored according to rupture time with respect to the mainshock. The gray star marks the 2021 Nippes epicenter from this study.

2.8 km/s, with two areas of larger slip that correspond to the two aftershock clusters described above. The first area of large slip, to the east, is ~30 km long, with largely dominant reverse motion between 0 and 12 km depth. The second area of large slip, to the west, is limited to shallow depth (0 to 4 km) with pure left-lateral motion. The source time function indicates a rupture duration of ~20 s, followed by a small, separated, and less well-constrained burst near the western termination of the rupture. Teleseismic back-projection source imaging [see (8), section 7] yields first-order rupture characteristics consistent with the kinematic source inversion results, with a 50- to 60-km-long rupture propagating unilaterally westward at an average speed of ~3 km/s (Fig. 3D). This consistency relies on calibrating seismic ray propagation paths using aftershock data to account for local structure heterogeneity. The accuracy of the aftershock locations provided by citizen-based seismic stations was essential to ensuring the quality of the calibration.

We confirmed the seismic source mechanism using independent geodetic data available with a few weeks' delay [see (8), section 8]. Radar interferograms from the Sentinel 1 A and B and ALOS-2 satellites show substantial vertical motion in the epicentral area, consistent with thrusting on a north-dipping structure (Fig. 1B), and a rupture that reached the surface along the previously mapped Ravine du Sud fault (26) (Fig. 1B) but remained blind otherwise. A nonlinear least-squares search for the rupture geometry considering two rectangular fault planes [see (8), section 9] found that best-fit planes that coincide with the two aftershock clusters described above (Figs. 1B and 3A). A north-dipping (~60° north) plane in the eastern part of the epicentral region shows a combination of reverse and strike-slip motion, with a surface trace that coincides with the Enriquillo fault. A steeper (~71° north) north-dipping plane to the west shows mostly strike-slip motion, with a surface trace that coincides with the Ravine du Sud fault.

Given the coincidence between the nonlinear inversion rupture and the surface expression of the Enriquillo and Ravine du Sud faults, we used their mapped traces to build north-dipping rupture geometries at depth and infer the distribution of coseismic slip along them (Fig. 3C) [see (8), section 10]. The resulting interferometric synthetic aperture radar (InSAR) slip distribution is consistent with the rupture of two main patches, coinciding with the relocated aftershocks (Fig. 3A) and with the finite fault seismic model (Fig. 3B). This consistency highlights the value of RS data to rapidly assess the main characteristics of this earthquake sequence.

In the slip models, the main patch to the east coincides with the mainshock epicenter

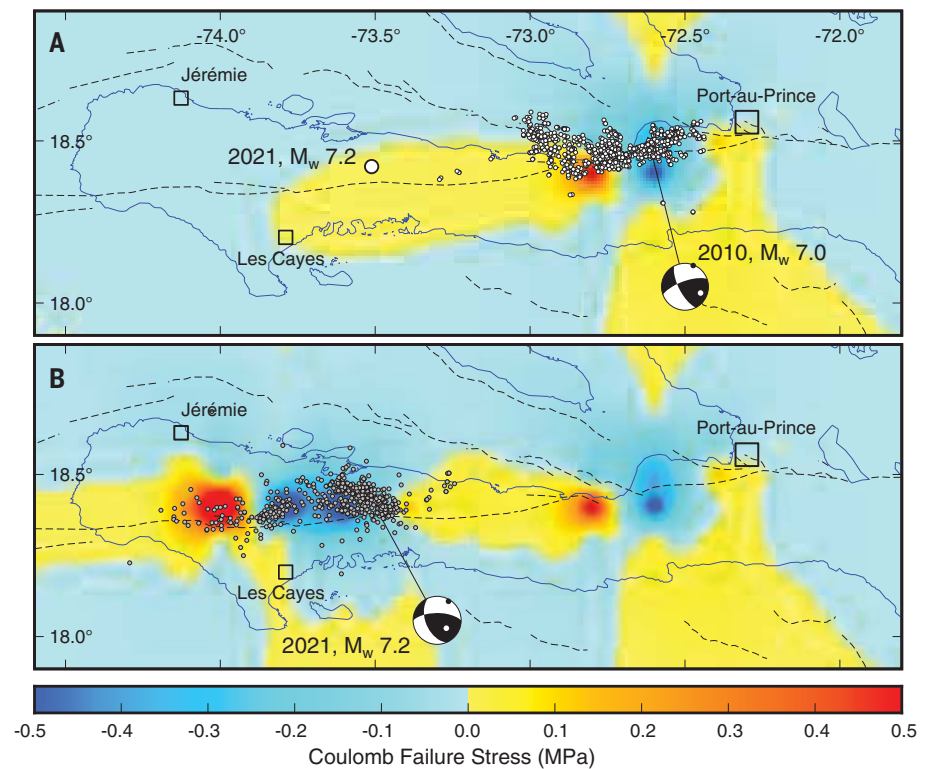


**Fig. 4. CFS on east-west trending, vertical strike-slip faults. (A)** CFS imparted by the 2010 earthquake, with its aftershocks shown as white dots. **(B)** CFS imparted by both the 2010 and 2021 earthquakes. The gray circles show the 2021 aftershock sequence as of 9 September 2021. The CFS is calculated at 5-km depth with a friction coefficient of 0.2.

location, with slip reaching 1.9 m, dominated by reverse motion. A second patch to the east coincides with the Ravine du Sud fault, with up to 2.3 m of purely strike-slip motion. The focal mechanisms corresponding to these two slip patches, highlighted by the aftershock distribution, are within uncertainties of those estimated independently from long-period modeling considering two point sources (Fig. 3C) [see (8), section 11].

We used this coseismic slip model, together with that of the 2010 earthquake (27, 28), to compute the Coulomb failure stress (CFS; Fig. 4) imparted on faults of similar orientation and kinematics, as the main, strike-slip Enriquillo fault [see (8), section 12]. The initiation area of the 2021 rupture falls within an area of increased CFS caused by the 2010 event, an indication that the two earthquakes may be part of a sequence in which the 2010 event triggered the 2021 earthquake, as observed on other major strike-slip fault systems. The aftershock distribution of the two earthquakes shows that their ruptures are not contiguous. The ~60-km-long fault segment between them, as well as other segments to the west and east, have not ruptured in a major earthquake since at least the series of four events in the 18th century (16), and show increased CFS (Fig. 4).

The 2010 and 2021 events have therefore increased earthquake hazard in southern Haiti, information critical to long-term planning for the region.

The 2021 Nippes earthquake bears similarities to the 2010 event (2, 3, 27, 28). Both earthquakes exhibited aftershocks and coseismic slip north of the Enriquillo fault, initiated with a substantial component of reverse faulting motion on an eastern segment, and propagated westward with later, mostly strike-slip motion. Their marked dip-slip moment release is intriguing given the mainly strike-slip motion recorded geologically on the Enriquillo fault, information hard-wired into Haiti's seismic hazard map (21). It is consistent, however, with interseismic geodetic measurements (11, 29, 30) (Fig. 1B) and onshore and offshore geophysical data (31–33) showing far-field kinematics combining strike-slip and convergence, with north-northeast/south-southwest-directed compression. A reappraisal of the seismic hazard map of Haiti is therefore needed to account for this substantial north-south shortening component and to provide updated information for building code purposes.

The rapid assessment of the source mechanism, near-field ground shaking, and aftershock distribution of the 2021 Nippes earthquake

was made possible by inexpensive seismometers hosted by citizens, together with information from classic seismological and geodetic data and models. The inclusion of the RS data in waveform inversions shows that they provide data of sufficient quality for adding valuable near-source information into the slip model, as confirmed by the InSAR slip inversion. This is an important example of a direct contribution of citizen seismology to understanding a large and damaging earthquake in the absence of conventional seismic stations in the near field of the event, highlighting the added value of citizen seismology for rapid earthquake response. The high benefit-to-cost ratio of citizen seismology makes it particularly relevant to regions of similar socioeconomic level as Haiti, where the implementation of conventional seismic networks operated by official institutions may be difficult (34).

## REFERENCES AND NOTES

- UN Office for the Coordination of Humanitarian Affairs, "Haiti: Tremblement de terre Rapport de Situation No. 2 Au 26 Août 2021" (OCHA, 2021); <https://reliefweb.int/report/haiti/ha-ti-tremblement-de-terre-rapport-de-situation-no-2-au-26-ao-t-2021>.
- E. Calais *et al.*, *Nat. Geosci.* **3**, 794–799 (2010).
- G. P. Hayes *et al.*, *Nat. Geosci.* **3**, 800–805 (2010).
- M. Hashimoto, Y. Fukushima, Y. Fukahata, *Nat. Geosci.* **4**, 255–259 (2011).
- E. Calais *et al.*, *Front. Earth Sci. (Lausanne)* **8**, 542654 (2020).
- R. E. Anthony, A. T. Ringler, D. C. Wilson, E. Wolin, *Seismol. Res. Lett.* **90**, 219–228 (2018).
- Ayiti-Séismes Project, "Prognosis on 08/23/2021 of the aftershocks of the Nippes earthquake, Haiti (08/14/2021, magnitude 7.2)" (Ayiti-Séismes Project, 2021); <https://ayiti.unice.fr/ayiti-seismes/>
- L. Fallou, E. Calais, A. Corbet, L. Hurbon, J. M. Théodat, "Citizen-seismology in Haiti, understanding citizens' interest and beliefs to enhance community resilience and contribute to risk reduction," paper presented at the Citizen Science SDG Conference: Knowledge for Change: A Decade of Citizen Science (2020-2030) in Support of the Sustainable Development Goals, Berlin, 14–15 October 2020.
- E. S. Cochran, J. F. Lawrence, C. M. Christensen, R. S. Jukka, *Seismol. Res. Lett.* **80**, 26–30 (2009).
- R. W. Clayton *et al.*, *Ann. Geophys.* **54**, 6 (2011).
- S. Symthe, E. Calais, J. B. de Chabaliar, R. Robertson, M. Higgins, *J. Geophys. Res. Solid Earth* **120**, 120 (2015).
- P. Mann, F. W. Taylor, R. L. Edwards, T. L. Ku, *Tectonophysics* **246**, 1–69 (1995).
- E. Calais *et al.*, *Geophys. Res. Lett.* **29**, 1856 (2002).
- P. Mann *et al.*, *Tectonics* **21**, 7–26 (2002).
- J. Scherer, *Bull. Seismol. Soc. Am.* **2**, 161–180 (1912).
- W. H. Bakun, C. H. Flores, U. S. ten Brink, *Bull. Seismol. Soc. Am.* **102**, 18–30 (2012).
- I. Bondár, E. R. Engdahl, A. Villaseñor, J. Harris, D. Storchak, *Phys. Earth Planet. Inter.* **239**, 2–13 (2015).
- C. Prépetit, "Anse-à-Veau, la ville sismique oubliée" (Bureau of Mines and Energy, Haiti, 2016); <http://www.bme.gouv.ht/uts/Anse-à-Veau.pdf>.
- European-Mediterranean Seismological Centre, "M 7.2 - HAITI REGION - 2021-08-14 12:29:09 UTC" (EMSC, 2021); <https://www.emsc-csem.org/Earthquake/earthquake.php?id=1023410#map>.
- F. Courboux *et al.*, *Seismol. Res. Lett.* **83**, 870–873 (2012).
- A. Frankel, S. Harmsen, C. Mueller, E. Calais, J. Haase, *Earthq. Spectra* **27** (L\_suppl), S23–S41 (2011).
- Ministère des Travaux Publics, Transports et Communications, "Code National du Bâtiment d'Haiti (CNBH) 2012" (MTP/TC, 2013); [https://www.mtpct.gov.ht/media/upload/doc/publications/CNBH\\_fusion.pdf](https://www.mtpct.gov.ht/media/upload/doc/publications/CNBH_fusion.pdf)
- US Geological Survey, "Search earthquake catalog" (USGS, 2022); <https://earthquake.usgs.gov/earthquakes/search/>
- A. Lomax, A. Savvaïdis, *J. Geophys. Res. Solid Earth* **127**, e2021JB023190 (2022).
- P. A. Reasenber, L. M. Jones, *Science* **243**, 1173–1176 (1989).
- N. Saint Fleur, N. Feuillet, Y. Klinger, *Tectonophysics* **771**, 228235 (2019).
- S. J. Symthe, E. Calais, J. S. Haase, A. M. Freed, R. Douilly, *Bull. Seismol. Soc. Am.* **103**, 2326–2343 (2013).
- R. Douilly *et al.*, *Bull. Seismol. Soc. Am.* **103**, 2305–2325 (2013).
- B. Benford, C. DeMets, E. Calais, *Geophys. J. Int.* **191**, 481–490 (2012).
- S. Symthe, E. Calais, *Tectonophysics* **679**, 117–124 (2016).
- J. Rodriguez, J. Havskov, M. B. Sørensen, L. F. Santos, *J. Seismol.* **22**, 883–896 (2018).
- D. Possee *et al.*, *Tectonics* **38**, 1138–1155 (2019).
- J. Corbeau *et al.*, *Tectonics* **35**, 1032–1046 (2016).
- S. Subedi, G. Hetényi, P. Denton, A. Sauron, *Front. Earth Sci. (Lausanne)* **8**, 73 (2020).

## ACKNOWLEDGMENTS

This project benefits from the collaboration of citizen seismologists in Haiti and the extra help of seismologists from Géoazur for manual picking of the aftershocks. J. Haase provided comments that improved an early version of the manuscript. ALOS-2 data

were provided from JAXA through the Earthquake Working Group coordinated by the Geospatial Information Authority of Japan and JAXA. We acknowledge seismic data from regional networks in the Dominican Republic, Cuba, Jamaica, and Alaska, and thank their operating agencies for making them available. **Funding:** This work was supported by the Centre National de la Recherche Scientifique (CNRS) and the Institut de Recherche pour le Développement (IRD) through their "Natural Hazard" program (E.C., S.S., T.M., B.D., F.C., J.P.A., J.C., A.D., D.B., S.P.); the FEDER European Community program within the Interreg Caraïbes "PREST" project (E.C., S.S., D.B.); Institut Universitaire de France (E.C., R.J.); Université Côte d'Azur and the French Embassy in Haiti (S.P.); the European Research Council (ERC) under the European Union's Horizon 2020 research and innovation program (grant no. 758210, Geo4D project to R.J. and grant no. 805256 to Z.D.); the French National Research Agency (project ANR-21-CE03-0010 "OSMOSE" to E.C. and ANR-15-IDEX-01 "UCAJEDI Investments in the Future" to Q.B.); the European Research Council (ERC) under the European Union's Horizon 2020 research and innovation program (grant no. 949221 to Q.B.); and HPC resources of IDRIS (under allocations 2020-AD011012142, 2021-AP011012536, and 2021-A0101012314 to Q.B.). **Author contributions:** E.C. designed and coordinated the study. S.S., S.S.F., and D.B. collected the citizen-seismology data. S.P., F.C., T.M., A.D., V.C., J.C., and F.P. collected the mainshock and aftershock bulletins. A.L. relocated the earthquake catalog. P.L. and Q.B. performed the ML-based aftershock detections. B.D. prepared the point source, linear, and kinematic models. J.P.A. analyzed the aftershock forecast. F.C. performed the RS50D spectral analysis. L.X. and L.M. prepared the source back-projection. R.J. and B.R. performed the InSAR analysis and resulting fault model. Z.D. performed the multiple point source solution. Y.F. processed the ALOS-2 interferograms. All authors wrote the original version of the manuscript. **Competing interests:** The authors declare no competing interests. **Data and materials availability:** All data and code used in this study are openly available. RADAR data can be obtained through ESA (Sentinel) or JAXA (Alos-2). Aftershock data can be obtained from <https://ayiti.unice.fr/ayiti-seismes/> (7). The codes used to process or model the data are published and public (8). The catalog of high-precision earthquake relocated with the NLL-SSST-coherence procedure (SM4) is available as supplementary data.

## SUPPLEMENTARY MATERIALS

[science.org/doi/10.1126/science.abn1045](https://doi.org/10.1126/science.abn1045)  
Materials and Methods  
Supplementary Text  
Figs. S1 to S26  
References (35–99)  
Data S1

3 November 2021; accepted 23 February 2022  
Published online 10 March 2022  
10.1126/science.abn1045